2010 IEEE International Conference on Robotics and Automation
Anchorage Convention District
May 3-8, 2010, Anchorage, Alaska, USA

FPGA-Based Adaptive Friction Compensation for Precision Control of Harmonic Drivers

Wen-Hong Zhu

Abstract— **FPGA (Field Programmable Gate Array) devices have emerged as a new type of reconfigurable high-performance computing hardware. Despite their successful applications in a variety of areas, FPGA devices are just about to find their way into the control systems. In this paper, a FPGA-based adaptive friction compensation scheme with a FPGA-based velocity estimator is reported for the first time. The FPGA device allows the LuGre friction model to be effectively implemented and updated at a clock rate. A parameter adaptation mechanism automatically accommodates the parameter uncertainties. To avert the need of having a division computation, which is extremely difficult if not impossible for a FPGA device to perform, a specially designed accumulator is used to create the velocity signal necessarily required for high-precision position tracking control. The developed technology is experimentally tested on a harmonic drive coupled with a brushless motor. The ratio of the maximum position tracking error to the maximum velocity reaches 0.00034 (s) - an unprecedented number in the precision control of harmonic drives.**

I. INTRODUCTION

Since being invented in 1980's, FPGA (Field Programmable Gate Array) devices have emerged as a new type of reconfigurable high-performance computing hardware with applications ranging from digital signal processing [1], speech recognition [2], image processing [3], computer hardware emulation [4], to aerospace and defence systems [5]. Despite being very successful in these aforementioned areas, FPGA devices, however, are just about to find their way into the control systems.

When control systems are concerned, FPGA devices possess both advantages and disadvantages over conventional CPU (Central Processing Unit) centered control systems. First, FPGA devices possess higher reliability, since they are logic electronics. Once being programmed, they keep working subject to the hardware component reliability, without the need to reset software. Second, FPGA devices make their clock signals available to control systems so that a FPGA-based control system can be updated at a rate up to the clock frequency that is much higher than the sampling rates of most CPU-centered digital control systems. Nonetheless, FPGA devices also possess disadvantages. The implementation of a FPGA design needs to be written in HDL (Hardware Description Language). The commercially available software (such as the System Generator by Xilinx Inc.) that converts graphic programming (such as Simulink) to HDL provides very limited design options and often results in a super-large HDL design beyond the hardware limit of a given FPGA device. In summary, FPGA-based control systems do possess advantages over CPU-centered control systems for these applications that require rapid state updates with limited computational complexity. Notable applications include, but are not limited to, friction compensations and servo control.

W.-H. Zhu is with the Spacecraft Engineering, Space Technologies, Canadian Space Agency, 6767 route de l'Aéroport, Saint-Hubert, QC, Canada J3Y 8Y9 Wen-Hong.Zhu@asc-csa.gc.ca

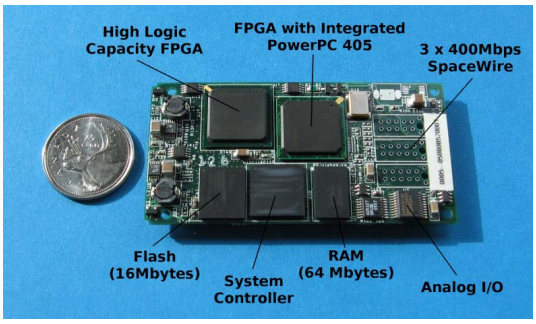

Fig. 1. The Q5 card with two FPGA devices (produced by Xiphos Technologies Inc.).

Friction compensation has been a long-term research topic in the precision servo control of mechatronic systems [6]. In robotic applications, harmonic drives are being widely used as driving mechanisms to make light-weight and compact robots. A typical harmonic drive includes a wave generator, a circular spline, and a flexspline placed in between [7]. While being compact in nature, a harmonic drive is inherently a deformable device associated with a large and dynamic friction. This characteristic makes the friction compensation of harmonic drives a thorny issue that, in turn, substantially challenges the control system design [8].

In this paper, a FPGA device as illustrated in Fig. 1 is used to implement an adaptive friction compensation scheme aimed at achieving the highest control precision of harmonic drives. The LuGre model presented in [9], [10] is used. The essence of the LuGre model is its inclusion of the dynamics of the so-called *bristle deflection*. While being simple, the LuGre model needs to be rapidly updated to well represent the friction physics. As a result, using a FPGA for LuGre model based friction compensation fully utilizes the advantages of the FPGA while avoiding its disadvantages.

As stated in [11], the LuGre model belongs to the class of *empirically motivated friction models*. In fact, the LuGre model captures the statistic behaviour of frictions without giving insightful details about the *asperity interactions* in a microscopic scale, leading to the existence of uncertainties in friction modeling. The friction uncertainties resulting from these asperity interactions can be interpreted as a parametric uncertainty associated with the LuGre model. Consequently, the need of using an adaptive mechanism to accommodate

this parametric uncertainty is motivated.

Accurate velocity estimation is crucial to the appropriate implementation of the LuGre model, since the only input to the LuGre model is the relative velocity between the two surfaces at which a friction occurs. Estimating a velocity with a theoretical zero phase-lag and an infinite bandwidth inevitably requires an acceleration measurement [12]. In applications where the reliability and the cost are concerned, using a position sensor (encoder) alone to estimate the velocity signal is always desirable. By far, the commonly used methods to estimate a velocity from a position measurement include the frequency count method and the period count method [13], [14]. The latter method requires an inverse calculation that converts the time period corresponding to each encoder pulse increment to the velocity signal. While being an easy task in CPU-centered control systems, the inverse calculation required in the period count method becomes extremely difficult, if not impossible, in FPGA implementation. In [15], a technology of using a counter driven by a frequency divider controlled by a look-up table was suggested to replace the inverse calculation. In this paper, an accumulator is used in the velocity estimator to replace the memory-consuming look-up table so that the entire velocity estimator that takes the advantages of both frequency count and period count methods can be effectively implemented in a FPGA device.

As will be seen blow, the FPGA-based adaptive friction compensation approach and the FPGA-based velocity estimation method constitute the two main contributions of this paper.

This paper is organized as follows: Section II presents the FPGA-based adaptive friction compensation scheme by incorporating the LuGre model. Then, the FPGA-base velocity estimation by using an accumulator is presented in Section III. In Section IV, both the FPGA-based velocity estimator and the FPGA-based adaptive friction compensation approach are implemented on a Xilinx Virtex-II FPGA device and tested experimentally on a commercially available harmonic drive coupled with a brushless motor, resulting in a trajectory tracking control result with an unprecedented accuracy.

II. ADAPTIVE FRICTION COMPENSATION

A. Position Control Objective

Let $x_d(t)$ be the desired position trajectory for all $t \in [0, \infty)$. The position control objective is to find a control variable $u(t)$ such that the actual position $x(t)$ tracks $x_d(t)$ asymptotically.

B. System Dynamic Model

The system dynamic model is described by

$$m\ddot{x}(t) + F(t) + d = u(t) \tag{1}$$

where m represents either a mass or a moment of inertia, d denotes a constant disturbance representing the bias of the Coulomb friction in different directions, $u(t)$ is the control variable, and $x(t)$ denotes the relative displacement between the two surfaces at which the friction occurs.

Remark 2.1: Eq. (1) represents the dynamics of either a point mass subject to a friction force or a motor rotor subject to a joint friction torque. When payloads are concerned, these payloads can be treated separately by using the *virtual decomposition control* approach [16], [17]. As a result, a payload related force/torque term will be added to the left hand side of (1).

C. The LuGre Friction Model

The LuGre model in continuous time can be expressed as [9], [10]

$$\dot{z}(t) = v(t) - \frac{\sigma_0 |v(t)|}{g(v)} z(t) \tag{2}$$

$$F(t) = \sigma_0 z(t) + \sigma_1 \dot{z}(t) + \sigma_v(v) \tag{3}$$

where $v(t) = \dot{x}(t)$ is the relative velocity between the two surfaces at which the friction occurs, $z(t)$ is an internal variable representing the *average deflection of the bristles*, $\sigma_0 > 0$ and $\sigma_1 > 0$ are two constants, $g(v)$ and $\sigma_v(v)$ specify the profiles of the Coulomb and Stribeck effects and the viscous friction, respectively, and finally $F(t)$ is the friction force/torque.

To properly accommodate the uncertainties associated with the friction model in the pre-sliding phase, (3) is re-written as

$$F(t) = \sigma[\sigma_0 z(t) + \sigma_1 \dot{z}(t)] + \sigma_v(v) \tag{4}$$

in which an uncertain parameter σ is added. Eqs. (3) and (4) are equivalent with $\sigma = 1$. The following assumption applies:

Assumption 2.1: Parameter $\sigma > 0$ is an unknown constant.

D. Adaptive Friction Compensation for Position Control

Given $x_d(t)$ and its first and second order time-derivatives $\dot{x}_d(t)$ and $\ddot{x}_d(t)$ for all $t \in [0, \infty)$, the required velocity and its time-derivative are designed as

$$\dot{x}_r(t) = \dot{x}_d(t) + \lambda[x_d(t) - x(t)] \tag{5}$$

$$\ddot{x}_r(t) = \ddot{x}_d(t) + \lambda[\dot{x}_d(t) - \dot{x}(t)] \tag{6}$$

where $\lambda > 0$ is a control parameter.

Then, let $z_r(t)$ be a (design) variable characterizing the required deflection of the bristles. The following dynamics are designed

$$\dot{z}_r(t) = v(t) - \frac{\sigma_0 |v(t)|}{g(v)} z_r(t) + \alpha(t)[\dot{x}_r(t) - \dot{x}(t)] \tag{7}$$

where $\alpha(t)$ is a time-variant control parameter to be specified later.

After having $z_r(t)$, the feedforward friction compensation term is design as

$$F_r(t) = \hat{\sigma}(t)[\sigma_0 z_r(t) + \sigma_1 \dot{z}_r(t)] + \sigma_v(v) \tag{8}$$

where $\hat{\sigma}(t)$ denote the estimate of σ in (4) and is updated by using the $\mathcal{P}$ function defined in [19, page:311] as

$$\hat{\sigma} = \mathcal{P}\left(s_\sigma, \rho_\sigma, \underline{\sigma}, \overline{\sigma}\right) \tag{9}$$

with

$$s_\sigma = [\dot{x}_r(t) - \dot{x}(t)][\sigma_0 z_r(t) + \sigma_1 \dot{z}_r(t)]. \quad (10)$$

In (9), $\rho_\sigma > 0$ is an update gain, and $\underline{\sigma} > 0$ and $\overline{\sigma} > 0$ denote the lower and upper bounds of σ, respectively.

Finally, the control variable is designed as

$$u(t) = \hat{m}(t)\ddot{x}_r(t) + F_r(t) + k_s[\dot{x}_r(t) - \dot{x}(t)] + \hat{d}(t) \quad (11)$$

where $k_s > 0$ is a control gain, and $\hat{m}(t)$ and $\hat{d}(t)$ denoting the estimates of m and d, respectively, are being updated by using the $\mathcal{P}$ function defined in [19, page:311] as

$$\hat{m} = \mathcal{P}(s_m, \rho_m, \underline{m}, \overline{m}) \quad (12)$$

$$\hat{d} = \mathcal{P}(s_d, \rho_d, \underline{d}, \overline{d}) \quad (13)$$

with

$$s_m = [\dot{x}_r(t) - \dot{x}(t)]\ddot{x}_r(t) \quad (14)$$

$$s_d = [\dot{x}_r(t) - \dot{x}(t)] \quad (15)$$

where $\rho_m > 0$ and $\rho_d > 0$ are two update gains, $\underline{m} > 0$ and $\overline{m} > 0$ denote the lower and upper bounds of m, and $\underline{d}$ and $\overline{d}$ denote the lower and upper bounds of d.

E. Stability Result

Theorem 1: The system described by (1), (2), and (4), subject to its control equations (5)-(15) under the following condition

$$\alpha(t) = \frac{\sigma_0 - \sigma_1 \frac{\sigma_0 |v(t)|}{g(v)}}{\beta} \quad (16)$$

is asymptotically stable for the position control, that is, $x_d - x \to 0$ when $t \to \infty$.

Proof: Let $\beta > 0$ be a constant, choose a non-negative function as

$$\begin{aligned} V(t) = & \frac{m}{2}[\dot{x}_r(t) - \dot{x}(t)]^2 + \frac{\sigma\beta}{2}[z_r(t) - z(t)]^2 \\ & + \frac{1}{2\rho_m}[m - \hat{m}(t)]^2 + \frac{1}{2\rho_d}[d - \hat{d}(t)]^2 \\ & + \frac{1}{2\rho_\sigma}[\sigma - \hat{\sigma}(t)]^2. \end{aligned} \quad (17)$$

After mathematical operations involving (1), (2), (4), and (5)-(16), it yields

$$\begin{aligned} \dot{V}(t) \leq & -[k_s + \sigma\sigma_1\alpha(t)][\dot{x}_r(t) - \dot{x}(t)]^2 \\ & -\sigma\beta\frac{\sigma_0 |v(t)|}{g(v)}[z_r(t) - z(t)]^2 \end{aligned} \quad (18)$$

leading to

$$\dot{x}_r(t) - \dot{x}(t) \in L_2 \bigcap L_\infty \quad (19)$$

$$z_r(t) - z(t) \in L_\infty. \quad (20)$$

Expression (19) further results in

$$\dot{x}_d(t) - \dot{x}(t) \in L_2 \bigcap L_\infty \quad (21)$$

$$x_d(t) - x(t) \in L_2 \bigcap L_\infty \quad (22)$$

in view of (5) and the $Lemma$ 1 in [20, page:1956].

Given bounded $\dot{x}_d(t)$ and $\ddot{x}_d(t)$, the boundedness of $v(t) = \dot{x}(t)$ is ensured from (21). Then, the boundedness of $v(t) = \dot{x}(t)$ ensures the boundedness of $g(v)$, the boundedness of $z(t)$ and $\dot{z}(t)$ from (2), the boundedness of $F(t)$ from (3), the boundedness of $z_r(t)$ from (20), and the boundedness of $\dot{z}_r(t)$ from (7) and (19). Furthermore, the boundedness of $v(t)$, $z_r(t)$, and $\dot{z}_r(t)$ leads to the boundedness of $F_r(t)$ from (8) and the boundedness of $u(t)$ from (6), (11), and (19). Finally, the boundedness of $u(t)$ and $F(t)$ implies the boundedness of $\ddot{x}(t)$ from (1), leading to the asymptotic stability in the sense of

$$\dot{x}_d(t) - \dot{x}(t) \to 0 \quad (23)$$

$$x_d(t) - x(t) \to 0 \quad (24)$$

from [21]. ■

Remark 2.2: When payloads are concerned, a payload related required (design) force/torque term will be added to the right hand side of (11). As a result, the asymptotic stability in the sense of (23) and (24) remains, in view of the *virtual decomposition control* approach [16].

III. FPGA-BASED VELOCITY ESTIMATION

A. Frequency Count and Period Count Methods

The frequency count method counts the number of encoder pulses occurred within a pre-specified sampling time period. Regardless of a variety of implementations, the velocity signal can be estimated by

$$v(k) = \frac{x(k) - x(k-1)}{T} \quad (25)$$

where $x(k)$ and $v(k)$ denote the position measurement by an encoder and the estimated velocity at the sampling time k, respectively, and T denotes the sampling period. The frequency count method is effective at high velocities, but insensitive at low velocities.

On the other hand, the period count method counts the time period corresponding to each encoder count increment by filling in a high frequency clock signal. The counted time period is then inversed to obtain the velocity estimation. In contrast to the first method, the period count method is accurate at low velocities, but ineffective at high velocities when the time period corresponding to each encoder count increment reduces to the scale of the clock signal period.

In on-chip implementation of the period count method, the most difficult task is to compute the inverse of the time period corresponding to each encoder count increment in order to obtain the velocity. The direct solution is to use a division calculation. While being effective for CPU-centered embedded microprocessors, this division computation is particularly difficult, if not impossible, for a FPGA implementation. In order to avert this division calculation, an US invention using two counters has been registered [15]. In this scheme, one counter counts the number of clock pulses upward to represent the time period. Another counter counts the velocity downward. A look-up table is used to adjust the down-counting rate of the velocity counter based on the reading from the time period counter. As a result, a trade-off

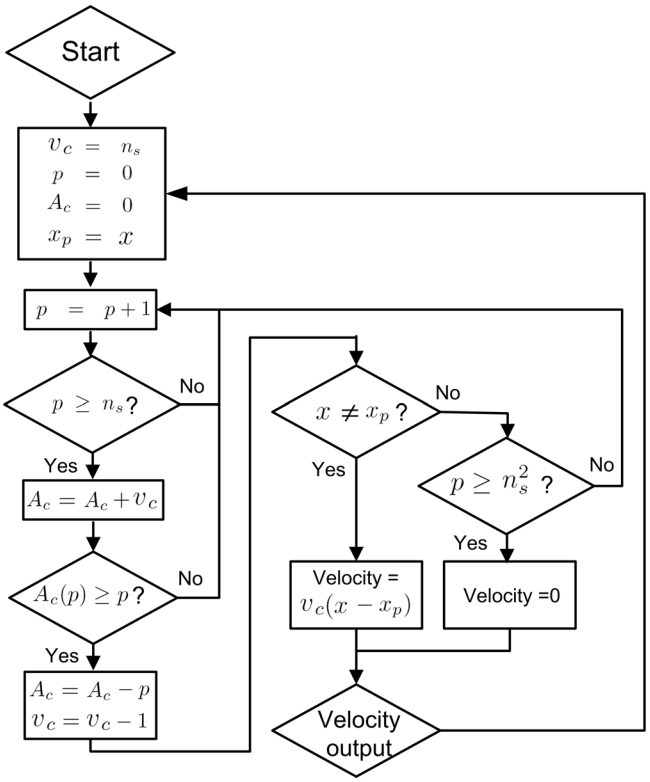

Fig. 2. Diagram of the velocity estimation approach.

between the complexity of the look-up table and the velocity counting accuracy must be made.

B. Proposed Solution with an Accumulator

With respect to the difficulty arisen from using a look-up table, a novel solution of using an accumulator is developed in this paper. The diagram is shown in Fig. 2.

This is basically a period count based approach with a limit being imposed on the minimum number of clock counts to be used. This number is $n_s \gg 1$.

In Fig. 2, a velocity counter v_c and a clock counter p are used. The counting mechanism is designed with an aim to make $v_c p$ as close to a constant integer ($\approx n_s^2$) as possible with its residual error being represented by the value of accumulator A_c. Note that $v_c \geq 0$ implies $A_c \geq 0$. Oh the other hand, this counting mechanism makes sure that $A_c \leq p$ holds after a counter correction. Therefore, the maximum counting error for v_c is to be limited by ± 1.

The clock counter limit number n_s plays a vital role to limit the maximum quantization error of the velocity estimate by

$$\delta_v \approx \frac{\delta_e}{n_s^2 T_c} \tag{26}$$

where δ_e is the encoder quantization error and T_c is the clock time period.

The final velocity estimation is given by $v = v_c\,(x - x_p)$, where x represents the current encoder reading and x_p the encoder reading at the last reset. This design makes sure that the estimated velocity can be either positive or negative. Furthermore, this counting mechanism permits the absolute value of $x - x_p$ to be larger than *one* for automatically performing the function of a frequency counter at high velocities.

IV. FPGA IMPLEMENTATION AND EXPERIMENTS

A. The Physical System

1) The Q5 Card: A Q5 card from Xiphos Technologies Inc. is illustrated in Fig. 1 in reference to a Canadian Quarter. There are two FPGA devices on the board. A Virtex-II - 1000 from Xilinx Inc. with a clock rate of 50 MHz is used to implement all the logic gates associated with both the velocity estimation and the adaptive friction compensation approaches. The other FPGA device functioning as a PowerPC 405 is not being used.

2) Harmonic Drive and Power Amplifier: A device FHA-11C-100 (from Harmonic Drive LLC) incorporating a harmonic drive with a brushless motor is used as the system to be controlled. This device has a gear ratio of 100 with a 2000-pulse quadrature encoder being attached to the motor shaft. This encoder gives a position resolution of $2 \times \pi/(100 \times 4 \times 2000) = 7.854 \times 10^{-6}$ (rad) at the output shaft. The brushless motor is driven by a power amplifier ZDR300EE12A8LDC from Advanced Motion Controls. Being configured in its motor torque control mode with a sampling time of 50 (μs), this power amplifier is driven by a DAC output channel associated with the Q5 Card [17], [18].

B. FPGA Implementation

1) Modification of (7) : To avoid the use of divisions in the control implementation, (7) is modified to

$$\dot{z}_r(t) = \frac{|v(t)|}{g^*}\left[\mathrm{sign}(v)g(v) - \sigma_0 z_r(t)\right] + \alpha^*[\dot{x}_r(t) - \dot{x}(t)] \tag{27}$$

where $g^* > 0$ and $\alpha^* > 0$ are two constant representing the nominal values of $g(v)$ and $\alpha(t)$, respectively.

Remark 4.1: The modification from (7) to (27) only affects the rate of the required *bristle deflection* $\dot{z}_r(t)$. This modification, however, does not change the steady state of the *bristle deflection* $z_r(t)$ in the sliding phase, which is characterized by $\sigma_0 z_r(t) \to \mathrm{sign}(v)g(v)$.

2) Friction Profile Determination: When in the sliding phase associated with $\sigma_0 z_r(t) \to \mathrm{sign}(v)g(v)$, $\dot{z}_r(t) \approx 0$, and $\hat{\sigma}(t) \approx 1$, it follows from (8) that $F_r(t) \approx \sigma_0 z_r(t) + \sigma_v(v) \approx \mathrm{sign}(v)g(v) + \sigma_v(v)$ holds. Without loss of generality, $v(t) > 0$ is assumed, leading to $F_r(t) \approx g(v) + \sigma_v(v)$. Let $g(v)$ be expressed by $g(v) = F_c + g_v(v)$ with $g_v(0) = 0$, where $F_c > 0$ denotes the Coulomb friction force/torque. Then, set control $u(t)$ in (11) as

$$u(t) = 0.75F_c + g_v(v) + \sigma_v(v) \tag{28}$$

and apply it to the system.

Remark 4.2: The reason of using the number 0.75 is to make sure that no over-compensation can occur during the friction profile determination process.

The principle behind the friction profile determination is that a constant payload under a constant residual friction

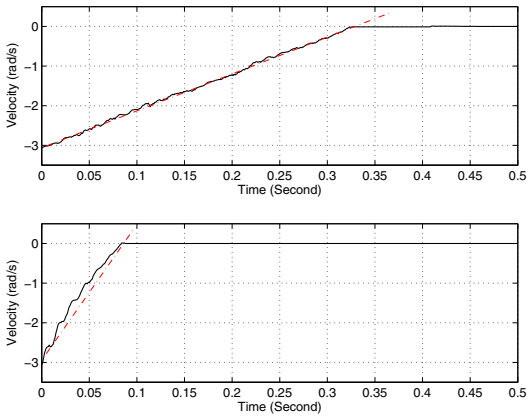

Fig. 3. Velocity responses with and without friction compensation by (28).

should produce a constant deceleration given an initial velocity. With this principle in mind, adjust both the structures and parameters of $g_v(v)$ and $\sigma_v(v)$ such that the deceleration of a given harmonic drive from a non-zero initial speed under control (28) becomes constant. As a result, the velocity profile of the constant deceleration is illustrated in the top figure of Fig. 3 and both $g(v)$ and $\sigma_v(v)$ are determined as

$$g(v) = \begin{cases} F_c + 3c_s v_s^2 - c_s v(t)^2 & \text{when} \quad |v(t)| \le v_s \\ F_c + 2c_s v_s^3 \frac{1}{|v(t)|} & \text{when} \quad |v(t)| > v_s \end{cases} \tag{29}$$

$$\sigma_v(v) = \begin{cases} [\sigma_2 + (\sigma_3 - \sigma_4 |v(t)|)] v(t) & \text{when} \quad |v(t)| \le \frac{\sigma_3}{\sigma_4} \\ \sigma_2 v(t) & \text{when} \quad |v(t)| > \frac{\sigma_3}{\sigma_4} \end{cases} \tag{30}$$

where $F_c > 0$ denotes the Coulomb friction force/torque, and $c_s > 0$ and $v_s > 0$ determine the profile of the Stribeck effect. In (30), $\sigma_2 > 0$, $\sigma_3 > 0$, and $\sigma_4 > 0$ are three parameters determining the profile of the viscous friction.

In Fig. 3, the two figures correspond to two cases by using (28) (the upper figure) and $u(t) = 0$ (the lower figure), respectively. The times needed to stop the two motions from the same initial velocity for the two cases is 0.326 second in the upper figure and 0.084 second in the lower figure. This suggests a $1 - \frac{0.084}{0.326} = 74\%$ friction compensation without encountering over-compensation.

C. Precision Position Control

A fifth order polynomial $6(p_f - p_0)(t/t_f)^5 - 15(p_f - p_0)(t/t_f)^4 + 10(p_f - p_0)(t/t_f)^3 + p_0$ is used to create the desired position trajectory, where p_0 and p_f denote the initial and final positions, respectively, and $t_f > 0$ denotes the time duration. This trajectory guarantees zero velocity and zero acceleration at both initial and final time instants.

Let $p_0 = 0$ (rad), $p_f = 0.1571$ (rad), and $t_f = 1$ (sec). The maximum velocity is 0.2945 (rad/s) occurred at $t = 0.5$ (sec).

The position tracking result is illustrated in Fig. 4. In the upper figure, the dashed red line represents the desired position and the solid black line represents the actual position. The position tracking error is illustrated in the lower figure. In Fig. 5, the parameter adaptation of $\hat{\sigma}(t)$ is shown in the upper figure, and the overall friction compensation torque $F_r(t)$ is shown in the lower figure.

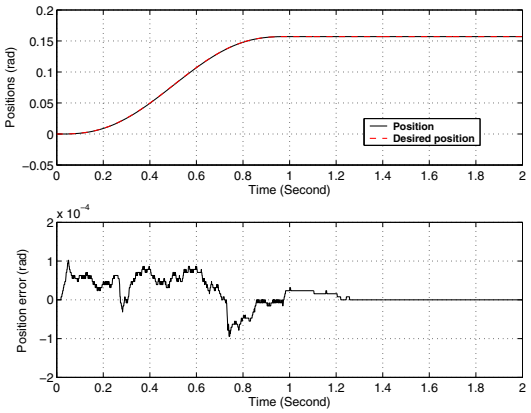

Fig. 4. Position tracking result and position error.

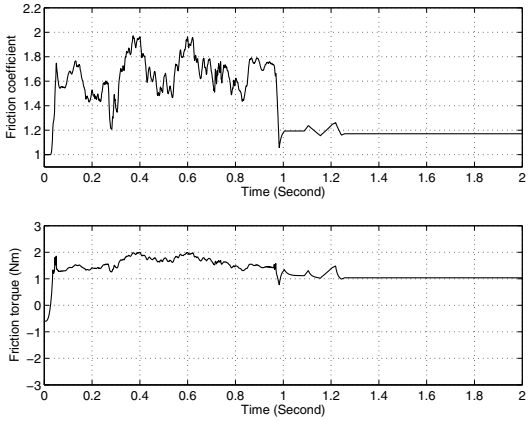

Fig. 5. Friction parameter $\hat{\sigma}(t)$ and friction torque $F_r(t)$.

In view of Fig. 4, the maximum position tracking error is about 1.0×10^{-4} (rad). Thus, the ratio of the maximum position tracking error to the maximum velocity reaches 3.4×10^{-4} (s).

D. Effect of Friction Parameter Adaptation

The effect of the adaptive friction compensation on the position tracking error is evaluated in Fig. 6. The four subplots correspond to $\hat{\sigma}(t)$ being updated by (9), $\hat{\sigma}(t) = 1.0$, $\hat{\sigma}(t) = 1.7$, and $\hat{\sigma}(t) = 2.44$, respectively. The parameter adaptation substantially reduces the position tracking error.

E. Performance Comparison

The position tracking control result obtained in this paper is compared to other results in previous publications, see Table I. The ratio of the maximum position tracking error to the maximum velocity is used as a performance indicator. Compared to a CPU-centered control system with a sampling rate of 1000 (Hz), the FPGA-based control reduces the performance indicator by a factor of five, suggesting that the control performance is improved $five$ times. This result also reveals that the FPGA-based control of harmonic drives can even surpass the control performances of a direct drive robot with a CPU-centered control system.

V. CONCLUSION

In this paper, a FPGA-based adaptive friction compensation approach has been developed for ultra precision control

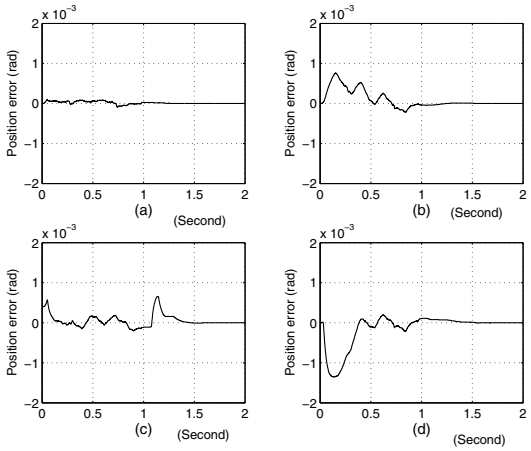

Fig. 6. Effect of the friction parameter adaptation on position tracking errors: (a) $\hat{\sigma}(t)$ is updated by (9); (b) $\hat{\sigma}(t) = 1.0$; (c) $\hat{\sigma}(t) = 1.7$; and (d) $\hat{\sigma}(t) = 2.44$.

TABLE I

PERFORMANCE COMPARISON.

Controller type	$\frac{\max \lvert e \rvert}{\max \lvert v \rvert}$ (s)
FPGA-based adaptive control for harmonic drive	**0.00034**
Adaptive control for harmonic drive in [22]	0.00170
Precision control of direct drive robot in [23]	0.00100

of harmonic drives. With the LuGre model, the parameter adaptation mechanism allows the natural uncertainties of the friction to be automatically updated at a hardware clock rate. An unprecedented position tracking result has been achieved in laboratory conditions. The ratio of the maximum position tracking error to the maximum velocity has reached 0.00034 (s). This result suggested that the proposed FPGA-based control can yield a substantial control performance improvement over a CPU-centered digital control system with the position tracking accuracy being increased by $five$ times.

VI. ACKNOWLEDGEMENTS

The author is grateful to Mr. Francesco Ricci at Xiphos Technologies Inc. for providing the photo of a Q5 card.

REFERENCES

[1] U Meyer-Baese, *Digital Signal Processing with Field Programmable Gate Arrays*, Springer, 2007.

[2] S. J. Melnikoff, P. B. James-Roxby, S. F. Quigley, and M. J. Russell, "Reconfigurable computing for speech recognition: preliminary findings," in *Field-Programmable Logic and Applications: The Roadmap to Reconfigurable Computing*, Springer Berlin, 2000.

[3] B. A. Draper, J. R. Beveridge, A. P. W. Bohm, C. Ross, and M. Chawathe, "Accelerated image processing on FPGAs," *IEEE Trans. Image Processing*, vol. 12, no. 12, pp. 1543-1551, 2003.

[4] J. Varghese, M. Butts, and J. Batcheller, "An efficient logic emulation system,", *IEEE Trans. Very Large Scale Integration (VLSI) Systems*, vol. 1, no. 2, pp. 171-174, 1993.

[5] H. B. Christophersen, W. J. Pickell, A. A. Koller, S. K. Kannan, and E. N. Johnson, "Small adaptive flight control systems for UAVs using FPGA/DSP technology," *AIAA 3rd "Unmanned Unlimited" Technical Conference, Workshop and Exhibit*, Chicago, Illinois, Sep. 20-23, 2004.

[6] J. Swevers, F. Al-Bender, C. Ganseman, and T. Prajogo, "An integrated friction model structure with improved presliding behavior for accurate friction compensation," *IEEE Trans. Automatic Control*, vol. 45, no. 4, pp. 675-686, 2000.

[7] T. D. Tuttle and W. P. Seering, "A nonlinear model of a harmonic drive gear transmission," *IEEE Trans. Robotics and Automation*, vol. 12, no. 3, pp. 368-374, 1996.

[8] W.-H. Zhu, "Precision control of robots with harmonic drives," *Proc. of 2007 IEEE Int. Conf. Robotics and Automation*, pp. 3831-3836, Rome, Italy, 2007.

[9] C. Canudas de Wit, H. Olsson, K. J. Aström, and P. Lischinsky, "A new model for control of systems with friction," *IEEE Trans. Automatic Control*, vol. 40, no. 3, pp. 419-425, 1995.

[10] K. J. Aström and C. Canudas de Wit, "Revisiting the LuGre friction model," *IEEE Control Systems Magazine*, vol. 28, no. 6, pp. 101-114, 2008.

[11] F. Al-Bender and J. Swevers, "Characterization of friction froce dynamics," *IEEE Control Systems Magazine*, vol. 28, no. 6, pp. 64-81, 2008.

[12] W.-H. Zhu and T. Lamarche, "Velocity estimation by using position and acceleration sensors," *IEEE Trans. Industrial Electronics*, vol. 54, no. 5, pp. 2706-2715, 2007.

[13] P. Bhatti and B. Hannaford, "Single-chip velocity measurement system for incremental optical encoders," *IEEE Trans. Control Systems Technology*, vol. 5, no. 6, pp. 654-661, 1997.

[14] G. Liu, A. A. Goldenberg, and Y. Zhang, "Precise slow motion control of a direct-drive robot arm with velocity estimation and friction compensation," *Mechatronics*, vol. 14, no. 7, pp. 821-834, 2004.

[15] C. J. Hasser, "Direct velocity estimation for encoders using nonlinear period measurement," US Patent 6,704,683 B1, 2004.

[16] W.-H. Zhu, Y.-G. Xi, Z.-J. Zhang, Z. Bien, and J. De Schutter, "Virtual decomposition based control for generalized high dimensional robotic systems with complicated structure," *IEEE Trans. Robotics and Automation*, vol. 13, no. 3, pp. 411-436, 1997.

[17] W.-H. Zhu and T. Lamarche, "Modular robot manipulators based on virtual decomposition control," *Proc. of 2007 IEEE Int. Conf. Robotics and Automation*, pp. 2235-2240, Rome, Italy, 2007.

[18] T. Lamarche and W.-H. Zhu, "A virtual decomposition control based communication network for modular robots applications," *Proc. of 16th Int. Conf. Computer Communications and Networks* (ICCCN 2007), pp. 1321-1326, Honolulu, Hawaii, USA, August 2007.

[19] W.-H. Zhu, and J. De Schutter, 1999, "Adaptive control of mixed rigid/flexible joint robot manipulators based on virtual decomposition," *IEEE Trans. Robotics and Automation*, vol. 15, no. 2, pp. 310-317.

[20] W.-H. Zhu and S. E. Salcudean, "Stability guaranteed teleoperation: an adaptive motion/force control approach," *IEEE Trans. Automatic Control*, vol. 45, no. 11, pp. 1951-1969, 2000.

[21] G. Tao, 1997, "A Simple Alternative to the Barbălat Lemma," *IEEE Trans. Automatic Control*, vol. 42, no. 5, p. 698.

[22] W.-H. Zhu, E. Dupuis, and M. Doyon, "Adaptive control of harmonic drives," *ASME J. Dynamic Systems, Measurement, and Control*, vol. 129, pp. 182-193, March 2007.

[23] W.-H. Zhu, H. T. Chen, and Z. J. Zhang, "A variable structure robot control algorithm with an observer," *IEEE Trans. Robotics and Automation*, vol. 8, no. 4, pp. 486-492, 1992.